Final Draft

of the original manuscript

Cano-Castillo, G.; Victoria-Hernández, J.; Bohlen, J.; Letzig, D.; Kainer, K.:

Effect of Ca and Nd on the microstructural development during dynamic and static recrystallization of indirectly extruded Mg–Zn based alloys.

In: Materials Science and Engineering A. Vol. 793 (2020) 139527.

First published online by Elsevier: 11.05.2020

https://dx.doi.org//10.1016/j.msea.2020.139527

Effect of Ca and Nd on the microstructural development during dynamic and static recrystallization of indirectly extruded Mg-Zn based alloys.

Guadalupe Cano-Castillo*, Jose Victoria-Hernández*, Jan Bohlen*, Dietmar Letzig, Karl Ulrich Kainer.

Magnesium Innovation Centre (MagIC), Helmholtz-Zentrum Geesthacht, Max-Planck-Str. 1, D-21502 Geesthacht, Germany.

* Corresponding authors
E-mail addresses: guadalupe.cano@hzg.de (Guadalupe Cano-Castillo), jose.victoria-hernandez@hzg.de (Jose Victoria-Hernández), jan.bohlen@hzg.de (Jan Bohlen).

Abstract

The present study examines the influence of Ca or Nd on the microstructure and texture modification during indirect extrusion and after subsequent annealing of Mg-Zn based alloys. The addition of such elements influence the recrystallization processes, i.e. dynamic (DRX) and static recrystallization (SRX), and leads to distinctive texture changes of samples extruded at different extrusion speeds. In the binary Mg-Zn alloys, the resulting texture after extrusion is the classical basal type texture, where there is an alignment of basal planes along the arc between the <10-10> and <11-20> poles. This development is independent of the extrusion speed, as the resulting microstructures are almost completely recrystallized. In the case of the Mg-Zn-Ca, there is a distinctive <10-11> component together with a <11-20> pole, while in the Mg-Zn-Nd alloy the so-called <11-21> rare-earth texture component and the <20-23> pole intensity are observed as DRX dominates the microstructural development. It is found that this distinctive behavior can be changed if partially recrystallized microstructures are subsequently annealed. This leads to an increase of the importance of SRX and a different resulting texture while maintaining a similar grain structure. Both recrystallization processes lead to different mechanical properties, yielding behavior and toughness as a result of the different texture development.

Keywords:

Magnesium, Microstructure, Texture, Dynamic recrystallization, Static recrystallization, EBSD, Mechanical properties.

1. Introduction

Nowadays, the use of light materials for diverse applications in the transportation industry has become inevitable in the world. In order to improve the fuel economy and/or enhance the utilization of batteries in electric vehicles, new lightweight structures need to be developed. In this regard, as the lightest structural metal, magnesium and its alloys are rather attractive. So far, some magnesium alloys have been used for diverse components in the automotive and aerospace industries [1]. This because of their high specific strength and stiffness. However, issues like low strength and high anisotropy still limit their extensive use. The high anisotropy arises from the fact that during processing the basal planes of the HCP structure of magnesium align parallel to the main forming direction [2]. The combined use of thermomechanical treatments, e.g. extrusion, and Mg alloy development can result in tailored microstructures, i.e.

small grain sizes, good distribution of secondary phase particles and crystallographic textures. With respect to extrusion processing conditions, e.g. the temperature, the extrusion ratio and the extrusion speed, can influence the recrystallization behavior and the development of the microstructure. Therefore, they have a strong effect on the texture and concomitant mechanical properties of the extruded materials. Furthermore, the texture development during processing is strongly influenced by the activation of different deformation and recrystallization mechanisms. The appropriate use of alloying elements like rare earths (RE) and Ca [3-8] also influences both mechanism type.

The appearance of distinctive texture components, e.g the so-called <11-21> RE-texture component, has been observed in Mg-RE containing alloys after extrusion processing [4]. Extruded Mg alloys, having textures in which the basal planes are not parallel to the main forming direction, have shown the ability to deform more extensively by basal <a> slip [9, 10]. This contribute with an enhancement of ductility and the reduction of the asymmetry of mechanical properties at room temperature [11, 12]. It has been reported that the formation of the rare earth (RE) texture is related with a change of the balance of active dynamic recrystallization (DRX) during thermomechanical processing, static recrystallization (SRX) and selective grain growth during subsequent annealing [13]

The additions of these rare earths on magnesium alloys have been studied in order to understand the mechanisms by which they modify the texture [4, 14-16]. Despite the low solubility of the specific case of the rare earth Nd [7] on the Mg-Zn system, different authors have found that still this element leads to weakening the texture even in low quantities [7, 12, 17]. Nevertheless, the exact mechanism that dominates the texture development is still on debate. Although Ca belongs to the non-rare earth alloying elements, the addition of this alloying element to Mg-Zn based alloys leads to the development of some characteristic texture components also resulting in a certain tilt of basal planes out of the extrusion direction [5, 18, 19]. This, despite the large atomic radius and relatively high solubility in magnesium of Ca [20]. A size misfit in the magnesium lattice structure or a decrease of the stacking fault energies are some of the features, which change the balance of deformation mechanisms in alloys modified by Ca [21, 22]. The changes in the grain structure and texture lead to an increase of the ductile behavior at room temperature of Mg-Zn-Ca alloys [6, 18].

Even though the mechanical behavior of Mg-Zn-RE and Mg-Zn-Ca seems to be similar, they develop some differences, especially in the grain structure and in the formation of certain texture components resulting after extrusion. Consequently, the aim of this study is to elucidate the effect of a changed recrystallization kinetics during extrusion and its impact on the microstructure and texture evolution of Mg-Zn based alloys with separate additions Ca and Nd. For this purpose, a variation of the extrusion speed (maintaining extrusion temperature and extrusion ratio constant) is investigated to reveal the differences resulting from DRX of these two alloying systems. The development of the different texture components as a result of changing this single extrusion parameter is analyzed by means of systematic electron backscatter measurements (EBSD). As in some extrusion trials (i.e. low extrusion speed) partly recrystallized microstructure have been found, further annealing is used to analyze the effect of SRX on these samples. The differences in the texture development and the impact on the mechanical properties are analyzed and the results are discussed in terms of the effect of texture modification by DRX or SRX.

2. Experimental procedure

Magnesium-zinc based alloys with separate additions of Ca and Nd were prepared by gravity casting. Hereafter, the alloys will be denoted as Z1 for the Mg-Zn, ZX10 for Mg-Zn-Ca and ZNd10 for the Mg-Zn-Nd. The chemical composition is shown in Table 1. Billets for indirect extrusion were prepared with a length of 150 mm and a diameter of 49 mm to fit the 50 mm container of extrusion press. Prior to extrusion, the billets were homogenized to get solid solution for 16 hours. The binary Mg-Zn alloy and the Ca containing alloy were homogenized at 400 °C while the Nd containing alloy was homogenized at 450 °C. The difference in temperature was due to the complexity to attain solid solution in the Nd containing alloy. Preheating the billets to the extrusion temperature, i.e 300 °C, was performed for 60 minutes. A constant extrusion ratio of 1:25 and ram speeds of 0.1, 0.6, 2.0, 5.0 and 7.5 mm/s were used to obtain round bars of 10 mm in diameter. The microstructure of the extruded bars was revealed by preparing the samples using the conventional metallographic methodology, starting with grinding up to 2500 SiC paper, polishing and finally using an etchant based on picric acid [23].

The average grain size (d) was determined from at least three different micrographs along longitudinal sections of each sample. The grain size was estimated using the computer software AnalySIS Pro™ that uses the linear intercept method. A more detailed microstructure and grain orientation analysis has been carried out using electron back scattered diffraction (EBSD). Sample preparation consisted of the use of standard metallographic techniques followed by electro polishing using an AC2 solution (Struers ™) at 30 V for 25 s at -20 °C. EBSD analyses were performed to measure the local orientation patterns using a field emission scanning microscope (Zeiss, Ultra 55, EDAX/TSL) on the longitudinal sections of the samples. The operation voltage was 15 kV and the used scanning step size was 0.45 µm. In order to understand the effect of static recrystallization on the microstructure and texture development, samples extruded to achieve partly recrystallized microstructure were subsequently annealed to fully recrystallized microstructures. The samples were annealed at 400 °C for diverse times followed by water quenching and were analyzed using optical microscopy and EBSD.

The texture measurements were carried out on polished samples in the transversal plane of the round bars. Pole figures (11-20), (0001), (10-11), (10-11), (10-12), (10-13) were measured up to a tilt angle of 70° using a Panalytical texture goniometer. Cu Kα radiation and a beam size of 1 mm^2 was used. Inverse pole figures were recalculated using an open-source code MTEX [24].

The mechanical behavior of differently recrystallized samples, i.e. dynamically recrystallized after extrusion and statically recrystallized using partly recrystallized sample, was evaluated. In order to avoid effects of grain size related hardening, the resulting microstructures of the annealed samples were tailored to be rather similar to the counterpart grain size of the DRX samples (i.e. Z1 alloy extruded at 0.6 mm/s, ZX10 alloy extruded at 2.0 mm/s, and ZNd10 alloy extruded at 5.0 mm/s). Samples for tensile tests were prepared with a diameter of 5 mm and a gauge length of 30 mm. Samples for compression test were prepared with a length of 13.5 mm and a diameter of 9.0 mm. Mechanical testing in tension and compression was carried out along the extrusion direction at room temperature using a 50 KN testing machine (Zwick Z050). A constant strain rate of 10^{-3} s^{-1} was used. At least three samples per condition were tested.

Table 1. Chemical composition of each alloy in wt%.

Alloy	Zn	Ca	Nd	Mg
Mg-Zn (Z1)	0.91	-----	-----	Bal.
Mg-Zn-Ca (ZNd10)	0.94	0.15	-----	Bal.
Mg-Zn-Nd (ZNd10)	0.98	-----	0.57	Bal.

3. Results and discussion

3.1 Grain structure evolution as a function of extrusion speed

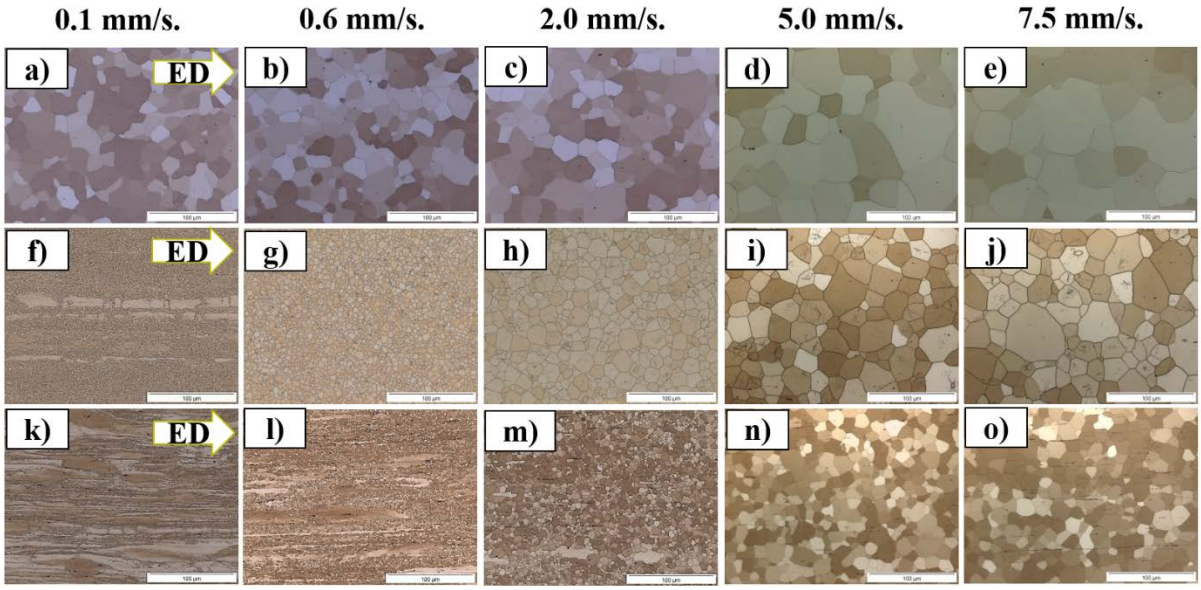

Figure 1. Optical micrographs at different extrusion speeds: a-e) Z1 alloy, f-j) ZX10 and k-o) ZNd10.

The micrographs from longitudinal sections after extrusion with varied extrusion speed of the three alloys are shown in Fig. 1. In comparison to the Z1 alloy, single additions of Nd and Ca into Mg-Zn based alloy have a significant effect on the microstructure development during extrusion. In one hand, Z1 exhibits recrystallized microstructures, where grain growth is observed as the extrusion speed increases (Figs. 1a-e). On the contrary, ZX10 (Figs. 1f-j) and ZNd10 (Figs. 1k-o) extruded at the low extrusion speeds exhibit partly recrystallized microstructures, observable in the form of large elongated grains with their long axis parallel to the extrusion direction. The amount of large elongated grains decreases with increasing extrusion speed. This leads to an increase on the fraction of the recrystallized microstructure. This is more pronounced in ZX10 where a fully recrystallized microstructure is obtained after extrusion at 0.6 mm/s (Fig. 1g). Conversely, in ZNd10 the unrecrystallized fraction of the microstructure remains up to an extrusion speed of 2.0 mm/s (Fig. 1m). Moreover, grain growth is also retarded in this alloy.
Zhang et al. [5] observed an increment of volume fraction of DRX grains and a grain growth phenomenon during the increase of extrusion speed of the Mg-5.3Zn-0.6Ca which is in agreement with the findings on the ternary alloys in the present work.

Fig. 2 depicts the average grain size of the recrystallized grains in each alloy as a function of the extrusion speed. In the grain size determination measurements, the large elongated grains were excluded and only equiaxed grains are taken into account and considered as recrystallized. A deeper analysis of recrystallized grains will be presented in the following sections of this article in the context of EBSD measurements. As depicted in Fig. 2, grain growth is more pronounced in the binary Z1 alloy as the extrusion speed increases. The grain growth kinetics decreases substantially in the ternary alloys compared to the binary alloy. Furthermore, from the tendency displayed in Fig. 2, it is clear that grain growht is more retarded in the presence of Nd rather than Ca, even at the highest extrusion speed used in this work. Such grain growth as the extrusion speed increases is associated to the deformation related heating. This can lead to a temperature difference between the initial billet temperature and processing temperature [25]. Moreover, it has been suggested that the net result in temperature increase is a linear function of the logarithmic ram speed [26]. Consequently, the deformation modes, DRX and subsequent grain growth are affected by the temperature, thus influencing the grain size [25]. This is consistent with the grain size increment in extruded bars as the extrusion speed increases, as shown in Fig. 2. Although Ca and Nd are effective alloying elements for preventing grain growth on the Mg-Zn alloys, the present study clearly shows that Nd is more effective in this regard than Ca.

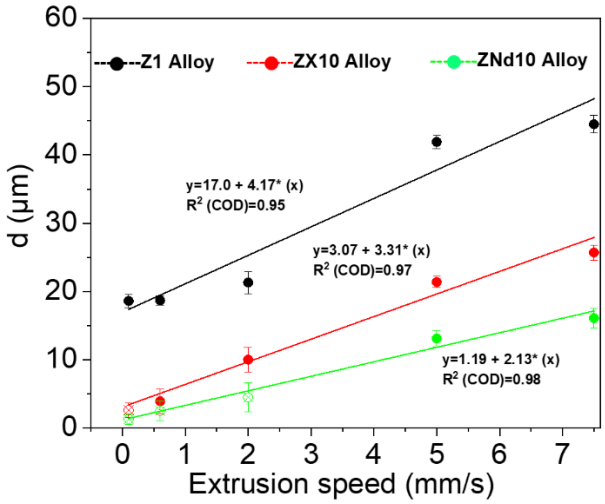

Figure 2. Average grain size as a function of extrusion speed for Z1, ZX10 and ZNd10 alloys. Measurements excluding the large deformed grains, especially at the lowest extrusion speed where partially recrystallized microstructures were found in the ternary alloys.

3.*2 Texture evolution as a function of extrusion speed*

Fig. 3 shows inverse pole figures in extrusion direction to reveal the texture evolution of the extruded bars as a function of the extrusion speed. For Z1 (Figs. 3a-e), there is a slight texture variation, especially in the texture intensity as the extrusion speed increases. Highest intensities are found at the <11-20> pole with a spread towards the <10-10> pole, there is a tendency of the <10-10> to be less significant with the extrusion speed. Such a texture orients basal planes mostly parallel to the extrusion direction and has often been reported for fully recrystallized extruded bars of magnesium alloys [27].

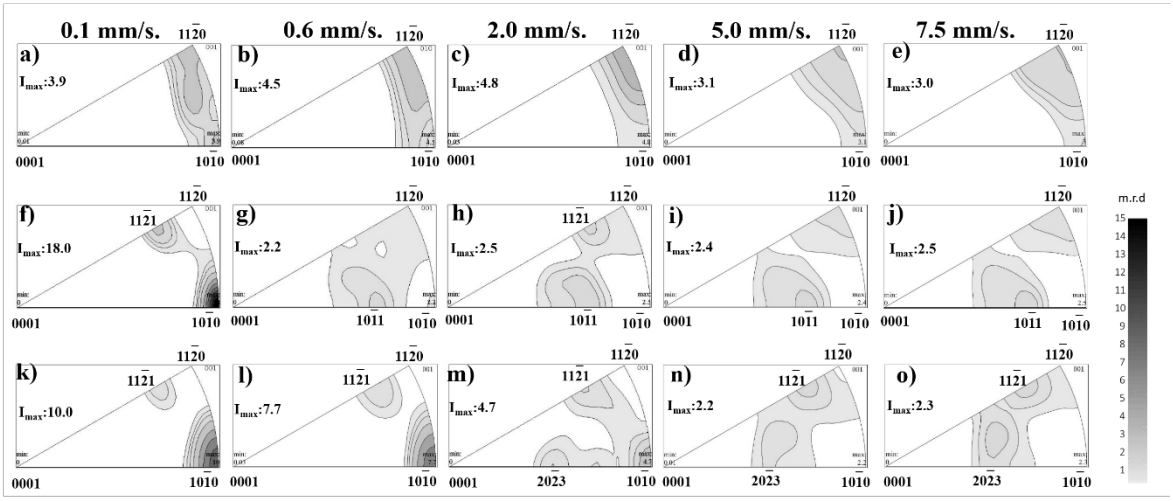

Figure 3. Texture evolution as a function of extrusion speed in Z1 alloy a-e), ZX10 f-j) and ZNd10 k-o). Inverse pole figures (IPFs) parallel to ED.

In the ternary alloys, different features in the texture evolution are observed. At the low extrusion speed, intensities at the <10-10> pole are dominating the textures (Figs. 3f and 3k), which vanish with increasing speed. While this also orients the basal planes parallel to the extrusion direction, such a fibre texture has been associated with the un-recrystallized fraction of the microstructur [9]. This latter aspect is in good agreement with the microstructure in Figs.1f and k. Furthermore, even after slow extrusion a further component is stablished with intensity in the vicinity of the <11-21> pole. This component is often observed in rare earth or calcium containing alloys [4].
If recrystallization is completed at higher speed, the texture is rather weak and the main texture component changes. In ZX10 the same component as in the binary alloy with intensity at the <11-20> pole is formed, see Figs. 3i-j. Furthermore, intensity seems to concentrate close to the <10-11> pole, thus maintaining the same tilt of basal planes out of the extrusion direction compared to the <11-21>-"rare earth" component, but with a rotation up to 30° around the c-axis, see Figs. 3g-j. With increasing speed this component is more pronounced. Unlike this, in ZNd10 intensity at the <11-21> pole is maintained up to the highest extrusion speed. A further pole develops with slightly higher tilt of the basal planes, shown as intensity at the <20-23> pole (Fig. 3m). However, the angular spread of the *c*-axis is not clearly distinguished from intensity at the <10-11> pole, which has been observed in ZX10.

3.3 *Impact of specific fractions of microstructure on texture evolution*

Fig. 4 depicts the EBSD orientation maps of all alloys after slow extrusion showing a separation of the unrecrystallized and recrystallized grains. The textures of the ternary alloys repeat the main finding of Fig. 3f and k, where the two components at the <10-10> and <11-21> poles are visible in both alloys, see Figs. 4b-c corresponding to the full EBSD maps. In order to observe possible hints of the origin of the pronounced components (observed in Figs. 3a, 3f and k) and highlight the orientations which are more resistant to dynamic recrystallization, a separation of fractions of the microstructure was carried out. The separation of the recrystallized and the un-recrystallized fraction of grains, is assisted based on a consideration of the internal orientation spread of grains, the grain orientation spread (GOS) [9, 28, 29].

It is assumed that recrystallized grains exhibit low in-grain misorientations as a result of a lattice free of dislocation which are an important source of such misorientations. On the other hand, grains which underwent plastic deformation and experienced active slip modes, would result in higher GOS. A GOS value of 1° as separator is considered in this work. In Fig. 4, the fraction of the microstructure corresponding to the small recrystallized grains (GOS<1°) in Z1 alloy there is a clear orientation tendency to the <11-20> pole while the ZX10 and ZNd10 alloys show a relatively weak texture, although they preserve their orientations mainly at the prismatic <10-10> pole (see Fig. 4a-c). Unrecrystallized grains in all alloys (GOS>1°) show the same <10-10> component which is significantly more pronounced. In ZX10, the rare earth texture component at the <11-21> pole is revealed in the un-recrystallized fraction (GOS >1°) of the microstructure but not in the fraction of recrystallized grains (GOS <1°), see Fig. 4b. In ZNd10, both fractions include grains with such orientation (Fig. 4c). It is believed that the element segregation modifies the grain growth kinetics, changing the components in the texture. This is the case for the Nd containing alloy, where the component <11-21> in the deformed condition with small DRX grains remain and preserve a certain grain growth uniformity. Such grain growth restrictions have been also linked with the appearance of the "rare-earth texture" in conventional AZ31 Mg alloy [30]. In AZ31 the grains with the basal planes parallel to ED normally grow unless a mechanism is active that changes the growth kinetics e.g. particles that restrict the grain growth. The grain growth tendency can be changed by particles in a way, that in recrystallized microstructures of AZ31 the <11-21> pole component can also be observed. On the contrary, in the Ca containing alloy there is not such a strong restriction to recrystallization and grain growth. As observed in Fig. 1, complete recrystallization occurred at lower extrusion speeds in ZX10 alloy in comparison to ZNd10. Thus, Ca also modifies the microstructure and texture in a slightly different way compared to the RE elements.

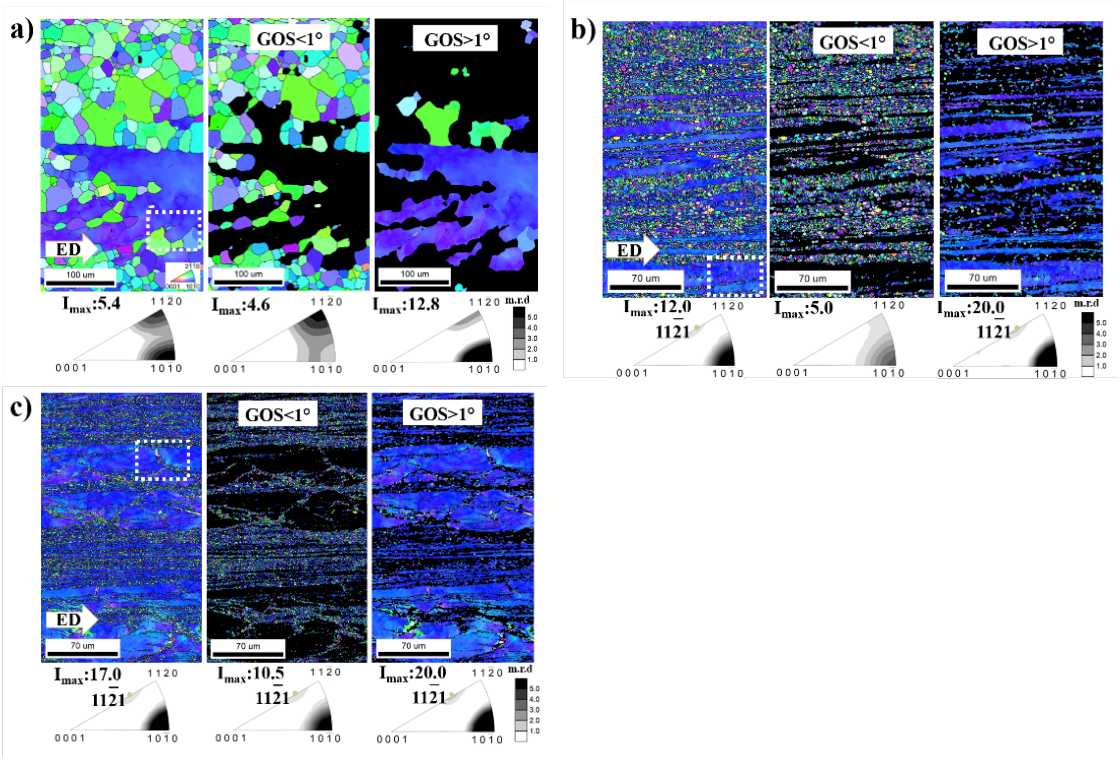

Figure 4. Inverse pole figure (IPF) orientation maps of samples extruded at 0.1 mm/s in a) Z1 alloy, b) ZX10 alloy and c) ZNd10 alloy.

3.4 *Dynamic recrystallization mechanism*

The different recrystallization kinetics in Z1, ZX10 and ZNd10 allows the systematical observation of microstructure and the related texture evolution. Especially important is to investigate possible nucleation sites of new dynamically recrystallized grains. It is important to mention at this point that the determination of recrystallization nuclei is hard using EBSD measurements and that investigations using transmission electron microscopy (TEM) is out of the reach of this work. However, it is possible to use results from EBSD measurements to distinguish small recrystallized grains (coming from possible nucleation sites). Due to the co-existence of deformed grains and new small DRXed grains, the microstructures from alloys extruded at low extrusion speed were selected. Fig. 5 exhibits a close up of those microstructures presented in the insets of Fig. 4. It is seen that in all three alloys (Fig. 5a-c) new recrystallized grains in the form of a necklace structure with varied orientations.
Moreover, substructures consisting of low angle grain boundaries (LAGB misorientation between 2 and 14°) are visible.
In the Z1 alloy, small and large recrystallized grains (marked with red triangle in Fig. 5a) exhibit some random orientation. Nevertheless, there is a tendency of most of the selected recrystallized grains to strengthen the <11-20> pole, while the deformed grains clearly show orientations towards the <10-10> pole. In the case of the ZX10 alloy presented in Fig. 5b, the much smaller recrystallized grains in comparison to the Z1 alloy show orientations still close to the <10-10> pole. There are still several recrystallized grains with orientation near the <11-20>, <11-21> and <10-11> poles. In this alloy, the deformed grains are also clearly oriented to the <10-10> pole. On the other hand, the ZNd10 alloy show a more distinctive behavior. While several new recrystallized grains are oriented close to the <10-10> pole, there are many that tend to be oriented along the arc between the <11-21> and <10-11> poles. Furthermore, some deformed grains are also located along this arc. This would mean that the balance of slip systems active during extrusion of the ZNd10 alloy is different in comparison to the ZX10 alloy. This can be related to the fact that recrystallization seems to be preferentially located along distinctive shear bands as depicted in Fig 4.
In order to differentiate the characteristics of deformed grains, which are in contact to new dynamically recrystallized grains, the internal misorientation along a line profile (see arrows in Fig. 5a-c) was plotted in Fig. 5d.
In non-recrystallized grains of Z1 alloy, the misorientation profile reveals a rather low misorientation alongside the measured distance, while in the ZX10 and ZNd10 alloys the line profiles reveal an increase of the misorientation in the non-recrystallized grains towards the grain boundary in contact to recrystallized grains. This indicates that the level of deformation contained in deformed grains, related to the internal misorientation of the ZX10 and ZNd10 alloys is significantly higher than those of Z1 alloy. The lower stored strain in the Z1 deformed grains can be a result of enhanced dynamic recovery as suggested in [29]. It is suggested that those grains are deformed preferential by prismatic <a> slip. Consequently, they are more resistant to recrystallization, in good agreement to [29]. On the other hand, the presence of alloying elements Ca and Nd can increase the resistance to dynamic recovery, thus storing more deformation inside the large elongated grains.

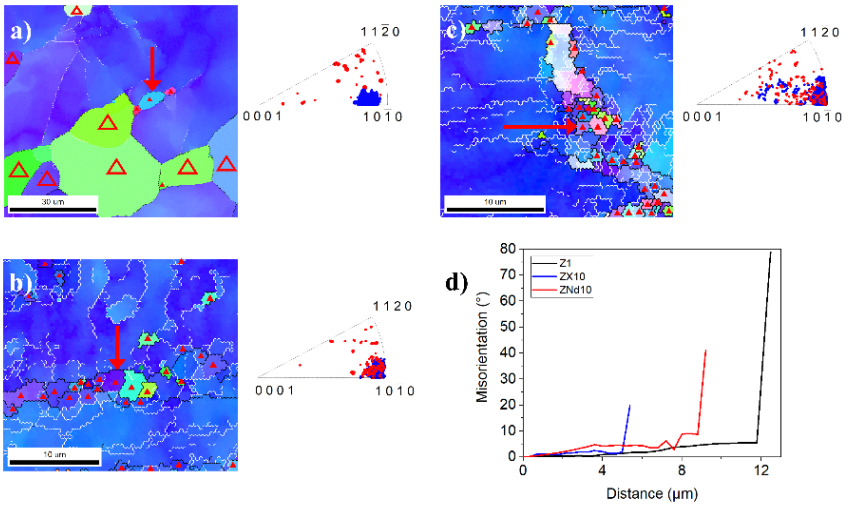

Figure 5. IPF maps and respective discrete inverse pole figure from insets displayed in Fig. 4 for a) Z1 alloy, b) ZX10 alloy and c) ZNd10 alloy. Fig. 5d plots the misorientation profile of deformed grains along the red line plotted in Figs. 5a-c. Red triangles denote recrystallized grains. In IPF maps black lines are high angle grain boundaries (HAGB θ>15°) and in white LAGB. Red dots in inverse pole figure refer to orientations of recrystallized grains while blue dots refer to orientations of deformed grains. (For interpretation of the references to color in this figure legend, the reader is referred to the web version of this article).

From enlarged areas depicted in Fig. 5a-c, it is seen that many sub-grains are developing towards the grain boundaries of deformed grains. Those sub-boundaries structures are also present in grains with GOS<1° considered in this study as recrystallized grains. This is consistent with the generation of new DRXed grains due to sub-grain formation based on a continuous dynamic recrystallization mechanism (CDRX)[30-32]. Only grains with high angle grain boundaries vary distinctly from this original orientation. Thus, it can be suggested that the balance between different types of recrystallization mechanisms, i.e. continuous (CDRX) and discontinuous (DDRX) types is slightly changed. This is related with the evolution of the dislocation density manifested as a continuous rotation of the LAGB until converted into HAGB [33, 34]. The grains are not so much different from the original orientation in this early stage, i.e. the onset of recrystallization. At this early stage, there is a certain tendency for the development of different texture components, which varies between the ternary alloys as discussed above. It is clear that ZNd10 alloy tend to form textures with intensity along the arc between the <11-21> and <10-11> poles even at the early stage of recrystallization. This tendency can be observed in both deformed and recrystallized grains as shown in Fig. 4.

3.4.1 *Effect of grain growth of the recrystallized fraction of the microstructure on texture development*

In order to differentiate the effect of different fractions and grain dependence of dynamically recrystallized microstructures, the fractions of dynamically recrystallized grains developed at low and intermediate extrusion speeds were evaluated.
The average grain size of recrystallized grains (d_{rec}) is considered as a limit to determine the effect of grain growth on the orientation development of such grains, thus separating small and large recrystallized grains. Fig. 6a and 6b show the recrystallized fraction of the microstructures of Z1 extruded at 0.1 mm/s and 0.6 mm/s, respectively. In this alloy both fraction of the grains show a spread of the grain between the <10-10> and the dominant <11-20> components.

There is a subtle trend to strengthen the <11-20> component as grain growth takes place. Figures 6c and 6e exhibit the recrystallized fraction of microstructures and respective textures after slow extrusion (0.1 mm/s) of the ZX10 and ZNd10 alloy respectively. This grain size consideration reveals a slight change compared to the deformation component in Fig.4 for ZNd10 and ZX10 alloys. In ZX10, the main orientation at the <10-10> pole is maintained but seems to be more pronounced in the smaller grains, see the texture in Fig. 6c, d_{rec} <3.0 µm. In the Fig. of d_{rec} >3.0 µm, potentially those with a growth advantage during recrystallization, an angular spread towards the <0001> pole (and therefore towards the <10-11> pole) is found. In ZNd10, no such grain size dependence is observed, both intensities at the <10-10> pole, and the <11-21> pole remain comparable, see Fig. 6e.

The effect of grain growth as a function of increasing the extrusion speed for ZX10 (2.0 mm/s) and ZNd10 (5.0 mm/s) alloy is depicted in Figures 6d and 6f, respectively. With grain growth by increasing the extrusion speed, the same separation of grains allows revealing that both alloys tend to develop intensity along the arc between the <10-11> and the <11-21> poles, which establishes a rotation of 30° around the c-axis. For ZX10, in the small grain size, there is no clear dominance between the intensities at the <10-11> and <11-21> poles, see texture in Fig. 6d, d_{rec} <11.0 µm. However, for the d_{rec} > 11.0 µm (Fig. 6d) the <10-11> pole is stronger. This indicates the importance of grain growth in the formation of the <10-11> component in the ZX10 alloy. For ZNd10, in the d_{rec} < 9.8 µm (Fig. 6f), it seems that the intensity at the <10-11> pole is somewhat higher, while with the d_{rec} >9.8 µm the <11-21> pole is more pronounced. Thus, the preference of grain orientations changes with the extrusion speed and the concomitant grain growth of recrystallized grains.
In each alloy, the texture evolution due to the grain growth during DRX recrystallization process is different. In Z1 alloy, the grains are principally spread between the prismatic poles <10-10> and <11-20>. The latter one is strengthened as grain growth of recrystallized grains takes place. Such behavior is modify if Ca or Nd is added to the Mg-Zn alloy systems. The <10-11> becomes more dominant in the Ca containing alloy as grain growth takes place, while in Nd containing alloy the coarse grains are mostly oriented towards the <11-21> component.

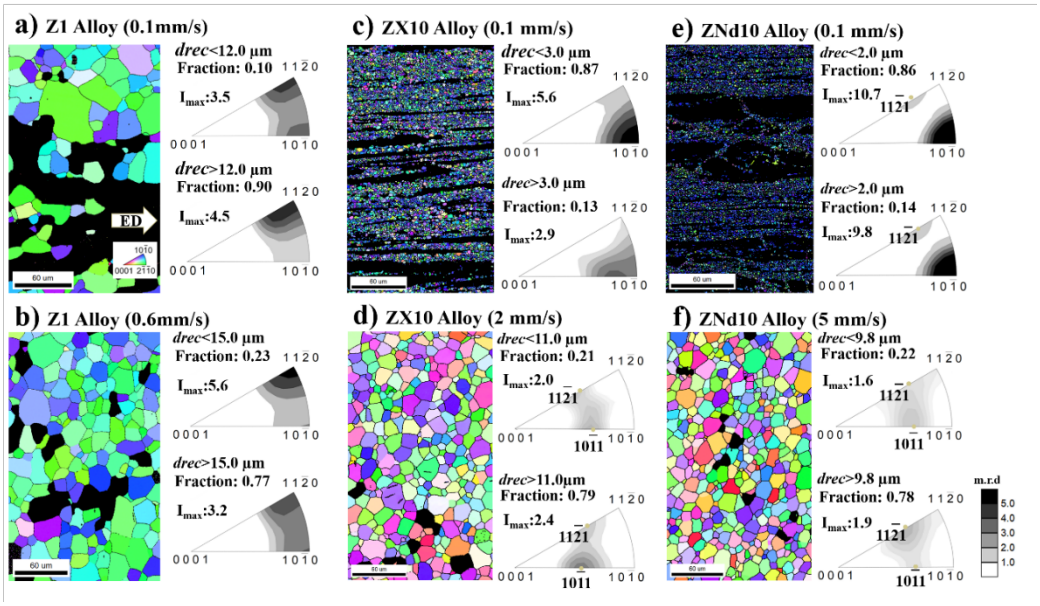

Figure 6. IPF maps of the recrystallized fraction of the microstructure (GOS<1°) and its texture analyzed as a function of the average recrystallized grain size: a) and b) Z1 alloy extruded at 0.1 and 0.6 mm/s, respectively; c) and d) ZX10 alloy extruded at 0.1 mm/s and 2.0 mm/s, respectively; e) and f) ZNd10 alloy extruded at 0.1mm/s and 5.0 mm/s, respectively.

3.5 *Static recrystallization mechanism*

After extrusion, the remaining heat during cooling down of the extruded bars is affecting the microstructure and texture, i.e. SRX is already activated but in an uncontrolled way. Such a change can be better explained using samples with partially recrystallized microstructures subjected to subsequent annealing. Then, in order to systematically determine the role of SRX on the texture development, partly recrystallized of samples from ZX10 and ZNd10 extruded bars at 0.1 mm/s were annealed. The analysis of Z1 is not presented due to the fact that no changes in the texture were found after SRX as a consequence of the high fraction of recrystallized microstructure found even in samples extruded at low speed.
The microstructures of samples from the ZX10 and ZNd10 alloys were tailored so the grain size of the SRX samples could be compared to grain structures of DRXed samples, i.e. samples extruded at 2.0 mm/s for ZX10 alloy and 5.0 mm/s for ZNd10 alloy.

The annealed microstructures of the ternary alloys revealed visible texture changes. Fig. 7 shows that after static recrystallization at 400 °C for 3.0 min in case of ZX10 (Fig. 7a) and 30 min for ZNd10 alloy (Fig. 7b), the texture is remarkably different to the counterparts dynamically recrystallized microstructures (c.f. Fig. 3h and 3n) despite the similar grain size. During SRX of the two alloys, intensity along the arc between the <10-10> and <11-20> poles is maintained. In ZX10, there are orientations with tilt out of the <10-10> pole, e.g. to the <20-21> pole, which also leaves basal planes with a tilt out of the extrusion direction, see Fig. 7a. A stronger alignment of basal planes along the arc between the <10-10> and <11-20> poles after static recrystallization is also visible on the ZNd10 alloy, Fig. 7b. Besides, there are orientations with varied tilt angle (e.g. at <20-23> pole).
The static recrystallization weakens the texture of the partly recrystallized samples but in essence, the grains maintain their orientation in the surrounding of the <10-10> pole in Ca and along the arc between the <10-10>-<11-20> poles in Nd containing alloy, i.e. they inherit the orientation of the dominant deformation texture component with the concomitant stronger recrystallization texture compared to the DRXed textures. At the end of static recrystallization, the basal planes remain aligned parallel to the ED.

Although the <11-21> RE component is present in the partly recrystallized microstructure (initial condition, Figs. 3f and 3k), in both alloys such component is suppressed after SRX. This is in agreement with Imandoust et al [35] for an Mg-Zn-Al-Mn-Y alloy where the RE grains disappear after the SRX process. It was explained that such behavior could be attributed to an isotropic grain growth process due to a grain boundary co-segregation effect that decreases the anisotropy in grain boundary energy and mobility. It is hypothesized in the context of the present work that the change of the balance of active deformation mechanisms as the temperature is increased as the extrusion speed increases. The importance of certain deformation mechanisms along with rapid growth of recrystallized grains (c.f. Fig. 6) could also influence the dominance of the RE-texture component.

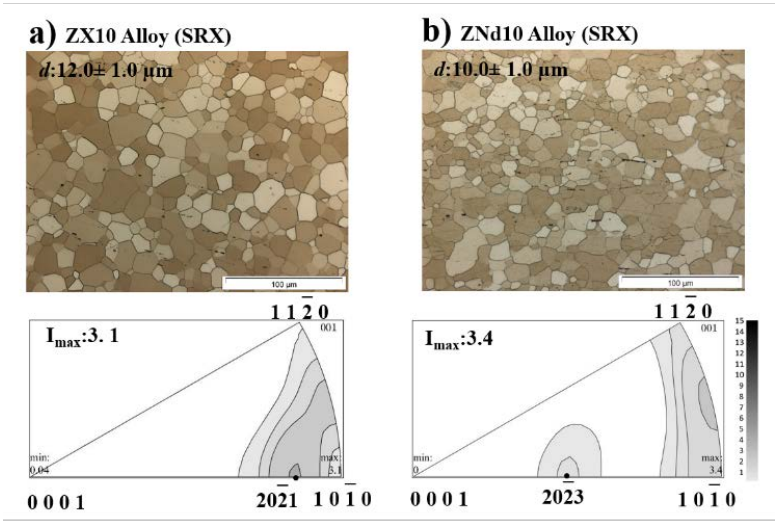

Figure 7. Microstructure and texture after static recrystallization (SRX) at 400 °C; a) ZX10 alloy for 3.0 minutes and b) ZNd10 alloy for 30 minutes.

A further analysis of static recrystallized microstructure using EBSD is shown in Fig. 8. The separation of the recrystallized fraction of the microstructure using the d_{rec} as a limit reveals that both alloys do not preserve or nucleate grains with the distinctive RE texture component (Figs. 8a and b). The texture remains similar at both considerations of the grain size, where the orientations are covering the <20-21> and <10-10> poles in ZX10, see Fig. 8a. Yet, there is a higher fraction of larger grains compared to grains smaller than the average grain size, that increases the intensity close to the <20-21> pole (Fig. 8a; d_{rec} >10.4 µm). Such a grain growth effect is also revealed in ZNd10, see Fig. 8b. There is a clear alignment of the basal planes parallel to ED and the <20-23> pole is only visible in grain sizes larger than the d_{rec}, i.e. 8.9 µm. The texture in ZNd10 shows an even stronger prismatic character with the complete suppression of the <11-21> component. The development of the <20-23> component is related with grains with certain grain growth advantages, as depicted in Fig. 8b. This also gives strength to the hypothesis given above, in which the increase of adiabatic heat in the regime of DRX could also increase the chance of activating additional deformation modes and enhance the preference of grain growth of grains having the <11-21> texture component. This latter aspect is under investigation.

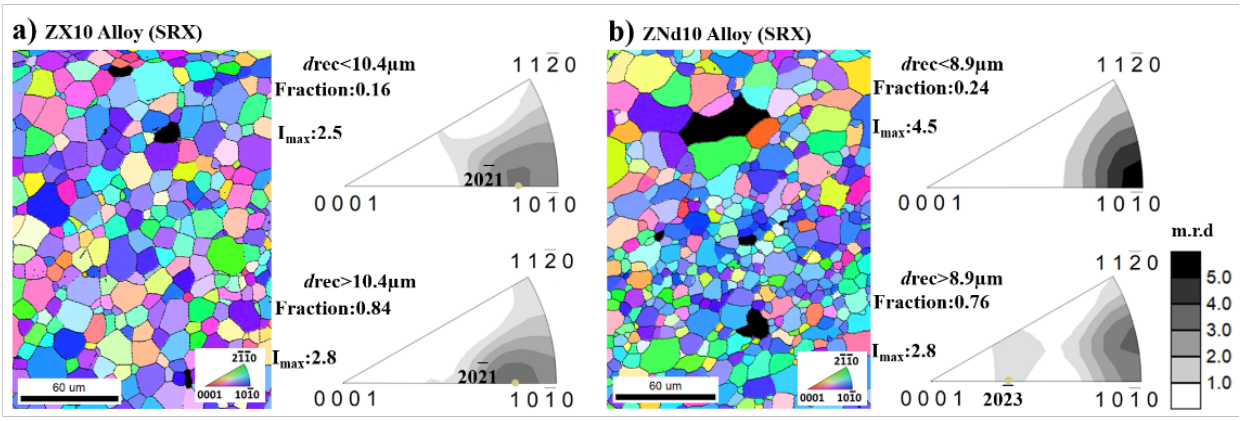

Figure 8. EBSD orientation maps and texture in a) ZX10 alloy treated at 400°C for 3.0 minutes and b) ZNd10 alloy heat-treated at 400°C for 30 minutes.

3.6 Mechanical behavior

The impact of different textures on the mechanical behavior of DRXed or SRXed samples with a similar grain size where analyzed in tension and compression. The mechanical behavior of the binary Z1 alloy is added. Typical true stress-strain curves from tensile and compression tests are shown in Fig. 9 for Z1, ZX10 and ZNd10 alloys. The mechanical properties, tensile yield stress (TYS), ultimate tensile stress (UTS), compressive yield stress (CYS), ultimate compressive stress (UCS) as well as fracture strain of the bars are presented in Table 2. Alloy Z1 extruded at 0.6 mm/s shows the well-known yield asymmetry where the yield stress in tension is significantly higher than in compression (Fig. 9a). Contrary to this, the alloys ZX10 and ZNd10 extruded at 2.0 and 5.0 mm/s, respectively, do not show such a behavior (see Figs. 9b and 9c, black lines). It is also observed that there is an increase of around 20 and 50 MPa of TYS for the SRXed alloys ZX10 and ZNd10, respectively. In these two cases, the microstructure develops from a partially recrystallized microstructure by means of SRX modifying the texture as explained above. Therefore, such and increase is a pure result of texture effects, since an increase of strength due to any Hall-Petch effects due to grain size can be discarded. On the other hand, it is observed that the CYS of both alloys are comparable to the counterparts DRXed samples.
The mechanical response and negligible yield asymmetry in the DRXed alloys can be explained with the alignment of the basal planes out of the ED, which makes mechanical twinning feasible in tension and compression.

The increase of TYS while maintaining the CYS leads to the yield asymmetry phenomena to be visible again in the SRXed samples. Such a behavior can be directly related with the texture that has a predominant character of the prismatic component, which makes the activation of mechanical twinning more difficult during tensile testing. The basal <a> slip is considered as the dominant deformation mechanism in the DRXed microstructure, thus further reducing the yield stresses in comparison to the SRXed microstructures. As discussed above, there is an increase of the yield stresses in tension as a result of the less twinning and basal <a> activity.

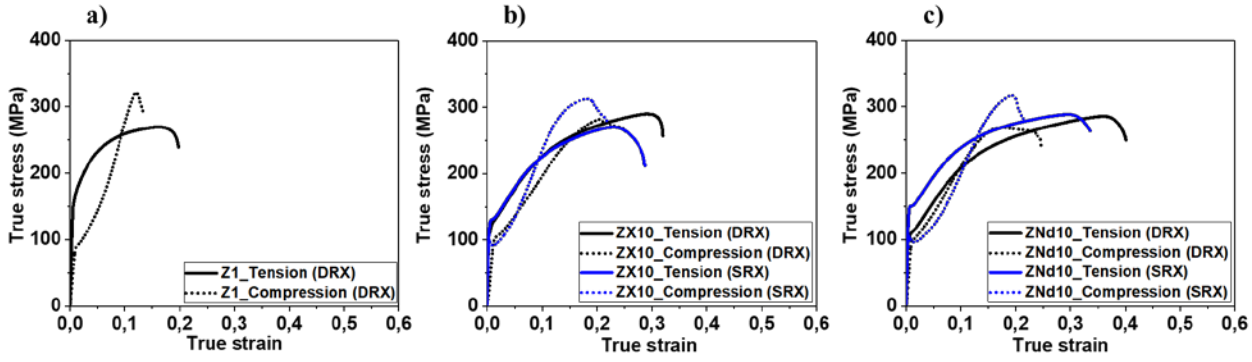

Figure. 9. True stress-true strain curves from tensile and compression tests: a) Z1 Alloy, b) ZX10 alloy, c) ZNd10 alloy.

Table 2. Mechanical properties measured parallel to the extrusion direction.

Alloy	TYS (MPa)	UTS (MPa)	Fracture strain	CYS (MPa)	UCS (MPa)	Fracture strain
Z1 (DRX)	154±1	263±1.0	0.20±0.01	90±1.0	318±4.3	0.10±0.01
ZX10 (DRX)	109±1	272±0.5	0.32±0.02	106±1	277±4.0	0.24±0.01
ZX10 (SRX)	129±2	268±1.0	0.29±0.01	101±2.5	311±2.5	0.21±0.01
ZNd10 (DRX)	101±2	262±2.0	0.40±0.02	101±1	268±1.0	0.23±0.01
ZNd10 (SRX)	150±1	272±1.0	0.32±0.02	107±1	320±4.0	0.21±0.01

In an attempt to further correlate the effect of texture due to the differences in DRX or SRX, the toughness in tension (U_T) and in compression (U_C) of the materials has been calculated. The values presented here, therefore, show the ability of the material to absorb mechanical energy in its unit volume [36, 37] and is calculated as follow in equation 1 and 2 [38].

$$U_T = [(TYS + UTS)/2] * \varepsilon_f \quad ----------(1)$$

$$U_C = [(CYS + UCS)/2] * \varepsilon_f \quad ----------(2)$$

Where ε_f corresponds to the fracture strain in tension or in compression. The results are depicted in Fig. 10. It shows that the absorbed energy in the tested samples of the Z1, ZX10 and ZNd10 is reduced from tension to compression.

The compared results in tension, shows that the Ca containing alloy absorbs a quite similar energy on both DRXed and SRXed samples, however in the Nd containing alloy the energy absorption is somewhat higher in the DRXed than SRXed samples. In the latter case, the higher ductility of the DRX sample is the reason for this difference. In compression, the absorbed energy is slightly higher in the DRXed than the SRXed samples of the Ca containing alloy, while a lower absorbed energy is observed in the DRXed samples compared to the SRXed samples of the Nd containing alloy.

As observed in Fig. 10, the difference in activity of deformation modes is also reflected in the small differences in the toughness of DRXed and SRXed samples. Despite the higher yield and ultimate tensile stresses recorded in SRXed compared to the DRXed samples, there is a decrease of the toughness, especially in the tensile samples. In one hand, this is related to the slightly lower ductility of the SRXed samples. On the other hand, it could be also related to the differences in the grain orientations which can affect the surface energy of the basal and non-basal planes of the samples depending on the direction of the applied load [39-41].

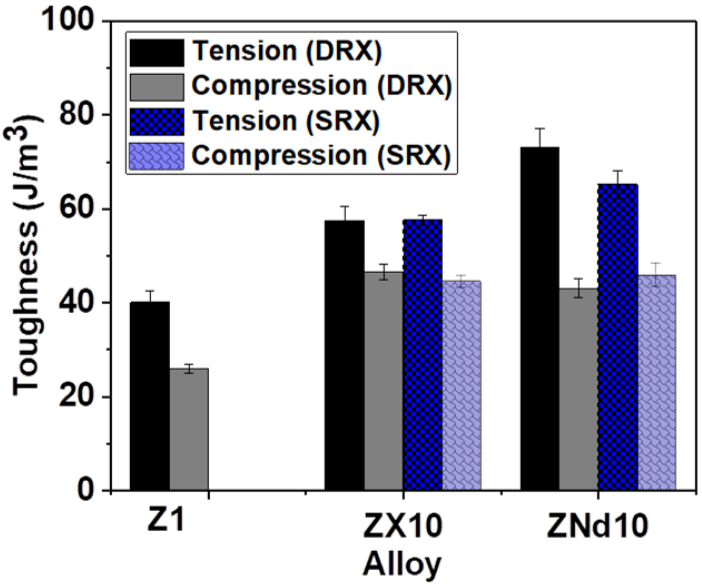

Figure. 10. Energy absorption in each material tested under tension and compression.

4. Conclusions

In this work, the effect of single additions of Ca and Nd on the evolution of microstructure, texture of Mg-Zn based alloys processed at different extrusion speed was analyzed. Special emphasis has been given in discussing the influence of DRX and SRX mechanisms on the texture development. In addition to this, the effect of different textures, while maintaining a comparable grain structure as a result of tailored annealing treatments, on the mechanical behavior was revealed. According to the results, we can draw the following conclusions:

1. Additions of Ca or Nd to the Mg-Zn based alloy influences significantly the recrystallization kinetics. In comparison, the Z1 alloy show no big influence of the extrusion speed on the grain structure and texture of extruded samples. In contrast, the recrystallization process is delayed in the ZX10 and ZNd10 alloys in comparison to the binary Z1 alloy. Higher extrusion speeds are needed to attained recrystallized microstructures in the ZX10 and ZNd10 alloys in comparison to the binary Z1.

2. There is a conventional development of the classical <10-10><11-20> texture in the binary Z1 independent of the extrusion speed. In the case of ZX10 alloy, the <10-11>-<11-20> poles become visible as DRX is completed at high extrusion speeds. In connection to higher fractions of recrystallized microstructures at higher speeds, the ZNd10 alloy exhibits the distinctive <11-21> -<20-23> poles.

3. The different impact on the texture development between DRX and SRX has been revealed. In the case of DRX in the Z1, recrystallized grains tend to orient to the <11-20> pole. This is strengthened as grain growth of recrystallized grains takes place. In the case of ZX10 alloy, the appearance of grains with orientations along the arc between the <11-21><10-11> poles only occurs in samples with higher fraction of recrystallized grains. Furthermore, grain growth of recrystallized grains seems to preferentially strengthen the <10-11> component.
In contrast, the <11-21> texture component is stable in the ZNd10 alloy in the extruded samples. This component is clearly strengthen as grain growth of recrystallized grains occurs.

With regard to annealing experiments to trigger SRX in partially recrystallized samples extruded at low extrusion speed, the results showed that the development of the <11-21> component was inhibited in both ternary alloys. Both alloys inherit the prismatic character of the deformed microstructure and there is a clear appearance of distinctive texture components. In ZX10 alloy is the <20-21> component while in the ZNd10 alloy the <20-23> component develops during subsequent annealing. Thus, a change in the balance of deformation mechanisms as well as the increase importance of grain growth of the recrystallized grains can be responsible for the different texture development in the DRX samples.

4. The mechanical properties are clearly influenced by the texture development during DRX and SRX. Yield asymmetry is obtained in the SRXed samples of ternary alloys that exhibit a texture where the basal planes are parallel to ED. This is attributed to a higher activation of twinning in compression. A reduction of the yield asymmetry is reached in ZX10 and ZNd10 samples with recrystallized microstructures produced by DRX. The orientation of the grains also affect other properties such as the toughness of the DRXed and SRXed samples. Yet, the combination of partly DRXed materials with SRX opens the possibility to influence the mechanical properties, e.g. increasing the TYS and UTS significantly in alloys that otherwise would show rather low TYS and UTS, e.g. in samples showing a dominant intensities along the arc between <11-21> and <10-11> texture components.

Acknowledgements

The authors would like to thank Günter Meister for his help with the casting of magnesium billets, Alexander Reichert for sample preparation and the technical assistance of Petra Fischer and Yukyung Shin for their help with EBSD measurements at Helmholtz-Zentrum Geesthacht. Guadalupe Cano-Castillo is grateful with the National Council of Science and Technology of Mexico (CONACyT) and the German Academic Exchange Service (DAAD) for funding which allows his research stay at the Helmholtz-Zentrum Geesthacht.

Credit Author Statement

GCC, JVH and JB contribute equally with the conceptualization, methodology, investigation and writing of the manuscript. DL and KUK contribute with the revision and discussion of the results. All approved the manuscript.
The authors declare not conflict of interest.

Data availability

The raw/processed data required to reproduce these findings cannot be shared at this time as the data also forms part of an ongoing study. Some results can be shared on reasonable request to the corresponding authors.

References

[1] I.J. Polmear, Magnesium alloys and applications, Materials Science and Technology 10(1) (1994) 1-16.
[2] J. Bohlen, S.B. Yi, J. Swiostek, D. Letzig, H.G. Brokmeier, K.U. Kainer, Microstructure and texture development during hydrostatic extrusion of magnesium alloy AZ31, Scripta Materialia 53(2) (2005) 259-264.

[3] J. Bohlen, M.R. Nürnberg, J.W. Senn, D. Letzig, S.R. Agnew, The texture and anisotropy of magnesium–zinc–rare earth alloy sheets, Acta Materialia 55(6) (2007) 2101-2112.
[4] N. Stanford, M.R. Barnett, The origin of “rare earth” texture development in extruded Mg-based alloys and its effect on tensile ductility, Materials Science and Engineering: A 496(1) (2008) 399-408.
[5] L.B. Tong, M.Y. Zheng, L.R. Cheng, D.P. Zhang, S. Kamado, J. Meng, H.J. Zhang, Influence of deformation rate on microstructure, texture and mechanical properties of indirect-extruded Mg–Zn–Ca alloy, Materials Characterization 104 (2015) 66-72.
[6] B.P. Zhang, L. Geng, L.J. Huang, X.X. Zhang, C.C. Dong, Enhanced mechanical properties in fine-grained Mg–1.0Zn–0.5Ca alloys prepared by extrusion at different temperatures, Scripta Materialia 63(10) (2010) 1024-1027.
[7] L. Ma, R.K. Mishra, L. Peng, A.A. Luo, W. Ding, A.K. Sachdev, Texture and mechanical behavior evolution of age-hardenable Mg–Nd–Zn extrusions during aging treatment, Materials Science and Engineering: A 529 (2011) 151-155.
[8] J. Victoria-Hernández, S. Yi, D. Klaumünzer, D. Letzig, Recrystallization behavior and its relationship with deformation mechanisms of a hot rolled Mg-Zn-Ca-Zr alloy, Materials Science and Engineering: A 761 (2019) 138054.
[9] J. Bohlen, S. Yi, D. Letzig, K.U. Kainer, Effect of rare earth elements on the microstructure and texture development in magnesium–manganese alloys during extrusion, Materials Science and Engineering: A 527(26) (2010) 7092-7098.
[10] E.A. Ball, P.B. Prangnell, Tensile-compressive yield asymmetries in high strength wrought magnesium alloys, Scripta Metallurgica et Materialia 31(2) (1994) 111-116.
[11] A. Imandoust, C.D. Barrett, T. Al-Samman, K.A. Inal, H. El Kadiri, A review on the effect of rare-earth elements on texture evolution during processing of magnesium alloys, Journal of Materials Science 52(1) (2017) 1-29.
[12] P. Hidalgo-Manrique, S.B. Yi, J. Bohlen, D. Letzig, M.T. Pérez-Prado, Effect of Nd Additions on Extrusion Texture Development and on Slip Activity in a Mg-Mn Alloy, Metallurgical and Materials Transactions A 44(10) (2013) 4819-4829.
[13] M. Huppmann, S. Gall, S. Müller, W. Reimers, Changes of the texture and the mechanical properties of the extruded Mg alloy ME21 as a function of the process parameters, Materials Science and Engineering: A 528(1) (2010) 342-354.
[14] N. Stanford, D. Atwell, M.R. Barnett, The effect of Gd on the recrystallisation, texture and deformation behaviour of magnesium-based alloys, Acta Materialia 58(20) (2010) 6773-6783.
[15] N. Stanford, D. Atwell, A. Beer, C. Davies, M.R. Barnett, Effect of microalloying with rare-earth elements on the texture of extruded magnesium-based alloys, Scripta Materialia 59(7) (2008) 772-775.
[16] J.P. Hadorn, K. Hantzsche, S. Yi, J. Bohlen, D. Letzig, J.A. Wollmershauser, S.R. Agnew, Role of Solute in the Texture Modification During Hot Deformation of Mg-Rare Earth Alloys, Metallurgical and Materials Transactions A 43(4) (2012) 1347-1362.
[17] B. Lv, J. Peng, Y. Peng, A. Tang, The effect of addition of Nd and Ce on the microstructure and mechanical properties of ZM21 Mg alloy, Journal of Magnesium and Alloys 1(1) (2013) 94-100.
[18] B. Zhang, Y. Wang, L. Geng, C. Lu, Effects of calcium on texture and mechanical properties of hot-extruded Mg–Zn–Ca alloys, Materials Science and Engineering: A 539 (2012) 56-60.
[19] M. Nienaber, K.U. Kainer, D. Letzig, J. Bohlen, Processing Effects on the Formability of Extruded Flat Products of Magnesium Alloys, Frontiers in Materials 6(253) (2019).

[20] I.-H. Jung, M. Sanjari, J. Kim, S. Yue, Role of RE in the deformation and recrystallization of Mg alloy and a new alloy design concept for Mg–RE alloys, Scripta Materialia 102 (2015) 1-6.
[21] S. Ganeshan, S.L. Shang, Y. Wang, Z.K. Liu, Effect of alloying elements on the elastic properties of Mg from first-principles calculations, Acta Materialia 57(13) (2009) 3876-3884.
[22] J. Zhang, Y. Dou, G. Liu, Z. Guo, First-principles study of stacking fault energies in Mg-based binary alloys, Computational Materials Science 79 (2013) 564-569.
[23] V. Kree, J. Bohlen, D. Letzig, K. Kainer, The Metallographical Examination of Magnesium Alloys, Praktische Metallographie/Practical Metallography 41 (2004) 233-246.
[24] F. Bachmann, R. Hielscher, H. Schaeben, Texture Analysis with MTEX – Free and Open Source Software Toolbox, Solid State Phenomena 160 (2010) 63-68.
[25] M. Shahzad, L. Wagner, Influence of extrusion parameters on microstructure and texture developments, and their effects on mechanical properties of the magnesium alloy AZ80, Materials Science and Engineering: A 506(1) (2009) 141-147.
[26] G. Liu, J. Zhou, J. Duszczyk, Finite Element Simulation of Magnesium Extrusion to Manufacture a Cross-Shaped Profile, Journal of Manufacturing Science and Engineering 129(3) (2007) 607-614.
[27] S. Yi, H.-G. Brokmeier, D. Letzig, Microstructural evolution during the annealing of an extruded AZ31 magnesium alloy, Journal of Alloys and Compounds 506(1) (2010) 364-371.
[28] C.D. Barrett, A. Imandoust, A.L. Oppedal, K. Inal, M.A. Tschopp, H. El Kadiri, Effect of grain boundaries on texture formation during dynamic recrystallization of magnesium alloys, Acta Materialia 128 (2017) 270-283.
[29] J. Victoria-Hernandez, S. Yi, J. Bohlen, G. Kurz, D. Letzig, The influence of the recrystallization mechanisms and grain growth on the texture of a hot rolled AZ31 sheet during subsequent isochronal annealing, Journal of Alloys and Compounds 616 (2014) 189-197.
[30] J. Victoria-Hernandez, S. Yi, D. Letzig, D. Hernandez-Silva, J. Bohlen, Microstructure and texture development in hydrostatically extruded Mg–Al–Zn alloys during tensile testing at intermediate temperatures, Acta Materialia 61(6) (2013) 2179-2193.
[31] F.J. Humphreys, M. Hatherly, Chapter 13 - Hot Deformation and Dynamic Restoration, in: F.J. Humphreys, M. Hatherly (Eds.), Recrystallization and Related Annealing Phenomena (Second Edition), Elsevier, Oxford, 2004, pp. 415-V.
[32] A.G. Beer, M.R. Barnett, Microstructural Development during Hot Working of Mg-3Al-1Zn, Metallurgical and Materials Transactions A 38(8) (2007) 1856-1867.
[33] S.E. Ion, F.J. Humphreys, S.H. White, Dynamic recrystallisation and the development of microstructure during the high temperature deformation of magnesium, Acta Metallurgica 30(10) (1982) 1909-1919.
[34] M.G. Jiang, C. Xu, H. Yan, S.H. Lu, T. Nakata, C.S. Lao, R.S. Chen, S. Kamado, E.H. Han, Correlation between dynamic recrystallization and formation of rare earth texture in a Mg-Zn-Gd magnesium alloy during extrusion, Scientific Reports 8(1) (2018) 16800.
[35] A. Imandoust, C.D. Barrett, T. Al-Samman, M.A. Tschopp, E. Essadiqi, N. Hort, H. El Kadiri, Unraveling Recrystallization Mechanisms Governing Texture Development from Rare-Earth Element Additions to Magnesium, Metallurgical and Materials Transactions A 49(5) (2018) 1809-1829.
[36] H. Pouraliakbar, M.R. Jandaghi, S.J. Mohammadi Baygi, G. Khalaj, Microanalysis of crystallographic characteristics and structural transformations in SPDed AlMnSi alloy by dual-straining, Journal of Alloys and Compounds 696 (2017) 1189-1198.
[37] H. Pouraliakbar, M.R. Jandaghi, Mechanistic insight into the role of severe plastic deformation and post-deformation annealing in fracture behavior of Al-Mn-Si alloy, Mechanics of Materials 122 (2018) 145-158.
[38] G.E. Dieter, D. Bacon, Mechanical metallurgy, McGraw-hill New York1986.

[39] H. Somekawa, T. Mukai, Effect of texture on fracture toughness in extruded AZ31 magnesium alloy, Scripta Materialia 53(5) (2005) 541-545.
[40] H. Somekawa, T. Mukai, Effect of grain refinement on fracture toughness in extruded pure magnesium, Scripta Materialia 53(9) (2005) 1059-1064.
[41] W. Hu, B. Zhang, B. Huang, F. Gao, D.J. Bacon, Analytic modified embedded atom potentials for HCP metals, Journal of Physics: Condensed Matter 13(6) (2001) 1193-1213.